Chemistry
A European
Journal

Chemistry Europe
European Chemical Societies Publishing

Accepted Article

Title: Phosphorescent k3-(N^C^C)-Gold(III) Complexes: Synthesis, Photophysics, Computational Studies and Application to Solution-Processable OLEDs

Authors: Hélène Beucher, Sudhir Kumar, Roopender Kumar, Estibaliz Merino, Wei-Hsu Hu, Gerrit Stemmler, Sergio Cuesta-Galisteo, Jorge Gonzalez, Leonard Bezinge, Jakub Jagielski, Chih-Jen Shih, and Cristina Nevado

To be cited as: *Chem. Eur. J.* 10.1002/chem.202003571

Link to VoR: https://doi.org/10.1002/chem.202003571

WILEY-VCH

10.1002/chem.202003571

WILEY-VCH

FULL PAPER

Phosphorescent κ^3-(N^C^C)-Gold(III) Complexes: Synthesis, Photophysics, Computational Studies and Application to Solution-Processable OLEDs

Hélène Beucher,[a]§ Sudhir Kumar,[b]§ Roopender Kumar,[a] Estíbaliz Merino,[a] Wei-Hsu Hu,[b] Gerrit Stemmler,[b] Sergio Cuesta-Galisteo,[a] Jorge A. González,[a] Léonard Bezinge,[b] Jakub Jagielski,[b] Chih-Jen Shih,[b]* and Cristina Nevado[a]*

[a] H. B., R. K.; E. M., S. C.-G., J. A. G., C. N.
Department of Chemistry
University of Zurich
Winterthurerstrasse 190, CH-8057, Zürich, Switzerland
[b] S. K., W.-H. S., G. S., L. B., J. J., C.-J. S.
Institute for Chemical and Bioengineering, Department of Chemistry and Applied Biosciences
ETH-Zürich
CH-8093, Zürich, Switzerland
§These authors contributed equally.

Supporting information for this article is given via a link at the end of the document

Abstract: Efficient OLED devices have been fabricated using organometallic complexes of platinum group metals. Still, the high material cost and low stability represent central challenges for their application in commercial display technologies. Based on its innate stability, gold(III) complexes are emerging as promising candidates for high performance OLEDs. Here, a series of alkynyl-, *N*-heterocyclic carbene (NHC)- and aryl-gold(III) complexes stabilized by a κ^3-(N^C^C) template have been prepared and their photophysical properties have been characterized in detail. These compounds exhibit good photoluminescence quantum efficiency (η_{PL}) of up to 33%. The PL emission can be tuned from sky-blue to yellowish-green colours by variations on both the ancillary ligands as well as on the pincer template. Further, solution-processable OLED devices based on some of these complexes display remarkable emissive properties (η_{CE} 46.6 cd.A^{-1} and η_{ext} 14.0%) thus showcasing the potential of these motifs for the low-cost fabrication of display and illumination technologies.

Introduction

Since the discovery of electroluminescence (EL)[1] and the first report of efficient low voltage EL in organic thin-film materials,[2] organic light-emitting devices (OLEDs) with small molecules or polymers as chromophores have risen as promising replacements for inorganic LEDs.[3] Two decades ago, seminal work by Forrest and coworkers showed that phosphorescent iridium(III) complex led to an important increase in the efficiency of organic electroluminescent devices.[4] Indeed, and in contrast to their fluorescent homologues, phosphorescent emitters have the capacity to harvest both minor singlet and major triplet excitons by intersystem crossing.[4,5] Due to the heavy nature of the metal[6] and the strong induced spin-orbit coupling, theoretically, internal quantum efficiencies of up to 100% could be achieved. This realization fostered extensive efforts focused on the design of transition-metal based-OLEDs containing iridium(III),[4,7] platinum(II),[8] osmium(II)[9] and ruthenium(II)[9] dopants. Iridium(III)-based phosphors are among the most attractive for the increasing flat-panel displays market,[10] owing to their ease of emission tunability over the entire visible spectrum.[7b,c,f,g] In fact, such metal-based OLEDs, deposited on polymers to enhance their flexibility, rank among the most efficient devices reported with high photoluminescence quantum yields (PLQY) and remarkable external quantum efficiencies (EQE) of 20 to 30%.[7a,f,8a,10]

In recent years, numerous studies have been published on the development of OLEDs using other metals, such as gold(III),[12] palladium(II)[13] and copper(I).[14] In the case of gold, research has lagged behind, probably because of the low-lying d-d states that result in a facile population of the $d_{x^2-y^2}$ orbital and effective non-radiative decay by thermal equilibration. Further, in certain cases, ease of decomposition of gold(III) complexes by reductive elimination has also played an important role.[15] Stability on gold(III) centers can be imparted by cyclometalation. Among others, the groups of Che and Yam have extensively exploited κ^3-(C^N^C) pincer ligands which, by introducing strongly σ-donating groups can push the dσ* orbital to higher-lying energy levels resulting in stable, phosphorescent gold(III) complexes.[16] Further, modulation of the electron-density, the steric hindrance and the π-conjugation of the pincer template and the ancillary ligand has been shown to fine-tune the color of emission from blue to red so that efficient devices with EQEs up to 23.8% could be obtained.[12d,e,16c,17]

In 2015, our group accomplished the assembly of novel κ^3-(N^C^C) pincer ligands that enabled the stabilization of the electrophilic gold(III) center and also the isolation and characterization of highly reactive intermediates postulated in gold-oxidative catalysis.[18] In contrast to its classical pincer κ^3-(C^N^C) analogue, our κ^3-(N^C^C)Au-Cl **1** displayed luminescence at 25 °C, with a promising PLQY of 17%.[18a] Thus, the novel κ^3-(N^C^C) template turned into a suitable platform to foster luminescence by increasing the chances of populating emissive states for gold complexes at high oxidation states. Interestingly, κ^3-(N^C^C)Au-F **2** and κ^3-(N^C^C)Au-alkynyl

10.1002/chem.202003571

complexes also displayed luminescence in solution at ambient temperature and showed intense vibronic-structured emission bands with the first peak maxima ranging from 489 to 497 nm. These emissions were assigned to a metal-perturbed ^{3}IL (π-π*) transition in the κ^3-(N^C^C) pincer. Further, they exhibit intense PLQY of up to 29% (Scheme 1).

Interestingly, a follow-up study of Yam and coworkers used an analogous κ^3-(N^C^C) scaffold to prepare solution-processable and vacuum-deposited OLEDs with EQE of up to 21.6%, and operational half-lifetime of up to 83.000 h at 100 cd.m^{-2}. Ancillary carbazole and thiolate ligands turned out to be preferred over alkynyl ones due to the increased stability of the corresponding bis-cyclometalated complexes.[19] Very recently, a second series of κ^3-(N^C^C)Au-carbazole complexes, where the N donor features an azole moiety, has also been reported.[20] In sharp contrast, our group has recently showed that careful selection of the alkynyl ancillary ligand can result in improved photophysical properties and also remarkable performance of the corresponding solution processed devices, with EQE of 16.2% and a maximum current efficiency (η_{CE}) of 56.4 cd.A^{-1} at 100 cd.m^{-2}.[21]

Based on these promising results, we report herein the synthesis and photophysical characterization of a variety of highly stable κ^3-(N^C^C)Au(III)-alkynyl, -NHC and -aryl complexes. These compounds display good PLQY in solution at 25 °C and can accomplish broad color-emission spectra, spanning from sky-blue to yellowish-green, by modulation of the electronic properties of the κ^3-(N^C^C) pincer and the ancillary ligand. These new species have also been computationally characterized and applied in solution-processable OLEDs, achieving good external quantum efficiencies (η_{ext}).

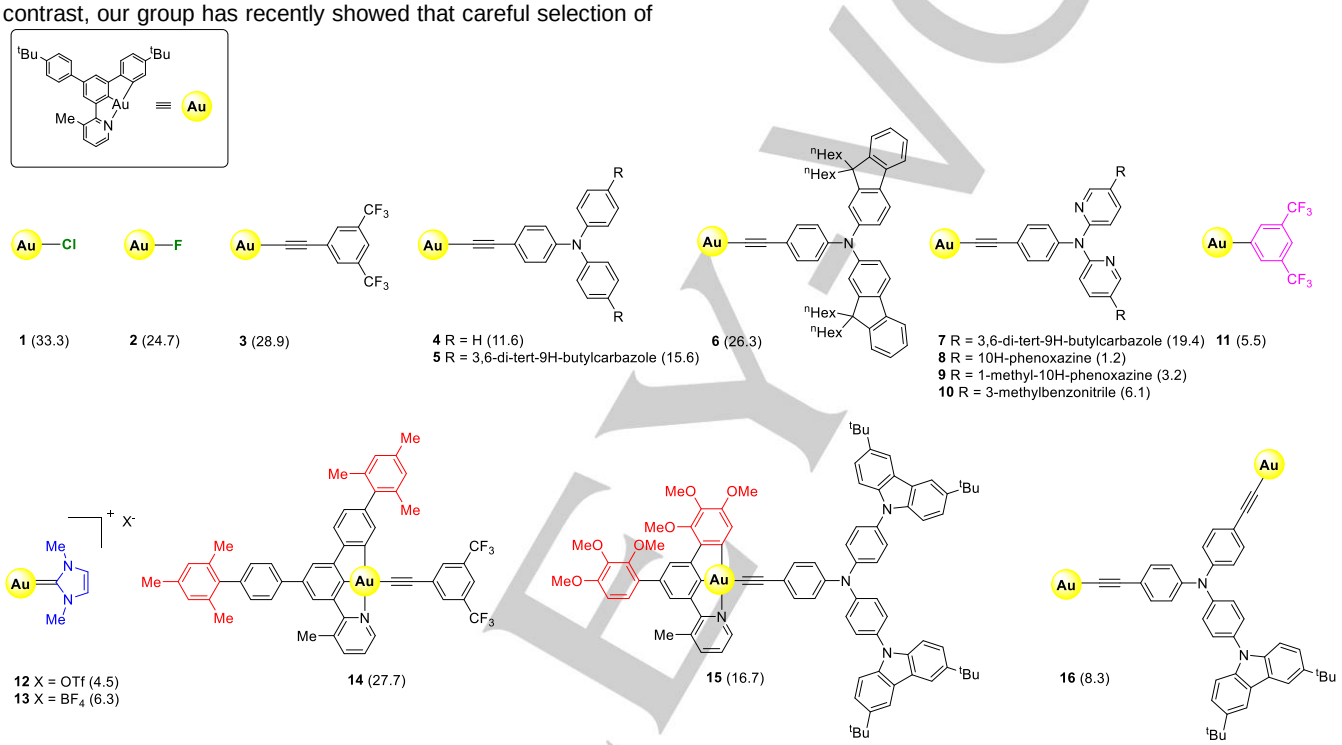

Scheme 1. Chemical structures of gold(III) complexes **1**-**16**. Quantum yields (%) were determined in a CH_2Cl_2 solution at 25 °C.

10.1002/chem.202003571

Results and Discussion

Design and synthesis of gold(III) complexes. Our design towards new κ^3-(N^C^C)gold(III) emitters was based on multiple criteria. On the one hand, we decided to use arylamines as good hole-injection/hole-transporting units and strong electron-donating groups (**4**-**10**, **15**-**16**). Carbazoles were also utilized as efficient carriers of positive charge (**5**),[22] whereas fluorenes were employed to rigidify the system and also to increase the solubility of the final complex by addition of long apolar alkyl chains at the Csp^3 center (**6**). In order to further explore the effect of different electronic features in our complexes, different heterocycles bearing both electron-donating (i.e. phenoxazine) as well as electron-withdrawing groups (i.e. cyanophenyl),[23] were prepared (**7**-**10**). Recently, arylacetylides have been shown to exhibit a low-lying highest occupied molecular orbital (HOMO), which might produce a non-radiative triplet ligand-to-ligand charge transfer (^{3}LLCT) excited state that competes with the emissive triplet intraligand (^{3}IL) one, thus resulting in lower PLQY.[16c] We set out to synthesize one example of gold(III)-aryl complex (**11**) to enable the comparison with the envisaged alkynyl analogues. To further extend the scope of this study, we wanted to prepare κ^3-(N^C^C)gold(III) complexes featuring NHCs (**12**-**13**), as the latter are known to be excellent σ-donating groups and have been described as prominent ancillary ligands to increase PLQY and excited states lifetimes in related systems.[16b] In addition, we aimed to tune the color of emission and improve the PLQY of our systems by varying the electronic properties and extending the π-conjugation of the pincer template (**14** and **15**).[16b,c,17a,c,h] Finally, we decided to investigate the effect of multinuclearity in these gold complexes (**16**). Tetra-gold(I) complexes bearing a pyrene tetraalkynyl connector have been reported by Poyatos and coworkers, displaying an intense fluorescence in solution with photoluminescence quantum efficiencies (η_{PL}) exceeding 90%.[24] To the best of our knowledge, only two such examples have been reported for gold(III), but the applications were focused on supramolecular studies,[25] rather than on the emissive properties.

The synthetic routes to complexes **1**-**16** are shown in Scheme 2.[26] All the complexes were isolated as solids and feature high decomposition temperatures (> 300 °C). Their structures were confirmed by ^{1}H, ^{13}C NMR and infrared spectroscopy as well as by high-resolution mass spectrometry and elemental analysis. Gold(III)-alkynyls **3**-**10** were synthesized, as depicted in Scheme 2A, by ligand exchange between the previously reported gold(III)-fluoride **2**[18a] and the corresponding free alkyne in the presence of triethylamine in dichloromethane (CH_2Cl_2) at 25 °C.[26] Alkyne diversification was carried out to explore the effect of the electronic and steric factors on the luminescence. Complex **11** was accessed by Au(III)/B transmetalation between **2** and the corresponding boronic acid in benzene (C_6H_6) at 80 °C, as indicated in Scheme 2B.[26] NHC complex **12** was prepared from **2** by mixing the corresponding silver carbene in CH_2Cl_2 at 100 °C for 2 hours protected from the dark.[26] Since the effect of the counter-anion can be crucial,[27] we also exchanged the triflate for a tetrafluoroborate group using the corresponding lithium salt to access **13** (Scheme 2C).[26] The synthesis of the pincer ligands in **14** and **15** was carried out following previously reported procedures and the alkyne units introduced according to the protocol described in Scheme 2A.[18a,26] Binuclear gold(III) complex **16** was prepared from **17** via Pd-catalyzed Sonogashira cross-coupling reaction followed by, Si-removal and ligand exchange with Au(III)-F **2**, as shown in Scheme 2D.[26]

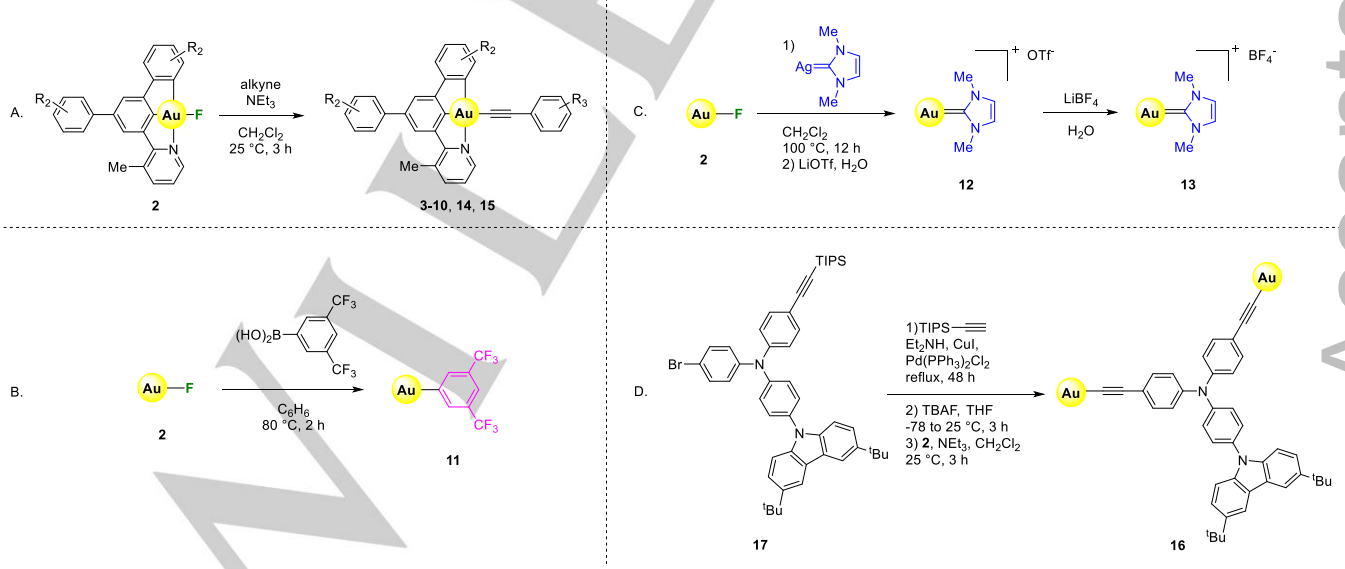

Scheme 2. Synthetic routes to gold(III) complexes **1**-**16**.

Photophysical properties. The ultraviolet-visible (UV-vis) absorption spectra for complexes **1**-**16** were measured in tetrahydrofuran (THF) at 298 K (Figure 1, blue trace). Most of the complexes show strong absorbance in the ultraviolet region which can be assigned to intraligand (IL) [$\pi\rightarrow\pi^*$] transitions both in the pincer and the ancillary ligands as well as LLCT [$\pi_{ancillary}\rightarrow\pi^*_{NCC}$]. We note a transformation of the corresponding vibronic absorption band into a single peak (red-shifted), when halogens (**1** and **2**) or electron-deficient alkynyl ligands (**3**) are replaced with the electron-donating aminophenylalkynyl substituents (**4**-**6**). Further, replacing the phenyl by a heteroaryl moiety in the aminoalkynyl motif (**7**-**10**) results in a slight blue shift but the shape of the band does not get affected. Similar absorption profiles to that observed for complexes **1**-**3** were obtained when NHC and aryl ancillary ligands were introduced as seen for complexes **11**-**13**. Varying the substituents on the pincer ligand (**14**-**15**) did not impact the spectra profile, even if a strong drop in the absorption band at 335-400 nm has to be pointed out in the case of **14**, likely due to the presence of an electron-deficient alkynyl moiety, as in the case of complex **3**. Moreover, **14** exhibits the smallest Stocks-shift ($\varepsilon = 1.84 \times 10^4$ dm^3.mol^{-1}.cm^{-1}) of gold(III) centered IL [$\pi\rightarrow\pi^*$] transitions among all complexes synthesized herein ($\varepsilon = 7.87 \times 10^4$ dm^3.mol^{-1}.cm^{-1}). Finally, binuclear complex **16** does not escape the trend established for aminophenylalkynyl derivatives and exhibits the same red-shifted single band in the absorption spectra. The optical energy band gaps of **1**-**16** were determined from the absorption edges, which are ranging from 2.87 to 3.05 eV (Table S1 in the Supporting Information).

The photoluminescence (PL) spectra of **1**-**16** were collected in a THF solution at 298 K using an excitation wavelength (λ_{ex}) of 365 nm (Figure 1, black trace). Both, single as well as multiple PL emission peaks ranging between 424 and 572 nm were recorded for these complexes. These bands can be assigned to the combination of ^{3}LLCT [$\pi_{ancillary}\rightarrow\pi^*_{NCC}$] and the metal-perturbed ^{3}IL [$\pi\rightarrow\pi^*$] transitions of the cyclometalated ligand, thus reflecting the structural diversity of these series. Further analysis of these transitions will follow in the computational section (vide infra).

The absolute η_{PL} of the complexes were recorded in degassed CH_2Cl_2 solutions at 25 °C. The η_{PL} values for complexes **1**-**16** range from 1.2 to 33.3% (see Scheme 1 and Table S1 in the Supporting Information). At first glance, it can be observed how complexes bearing halogens (**1** and **2**), (*bis*-trifluoro)phenylalkynyl (**3** and **14**) and (*bis*-fluorene)aminophenylalkynyl (**6**) groups as ancillary ligands display the highest luminescence within the entire series.

The phosphorescence spectra of complexes **1**-**16** were determined at 77 K in a nitrogen degassed glassy solution of 2-methyltetrahydrofuran (2-MeTHF). Compared to the PL spectra, a narrower spectral width was observed when halogen ligands were replaced together with a considerable blue-shift in phosphorescence spectra with two vibrational components around 490 and 520 nm for complexes **4**-**6**, **9** and **16**. (Figure 1, red trace). The triplet energies (E_T) of **1**-**16** were estimated from the second emission peak in the phosphorescence spectrum of each gold(III) complex. These complexes showed a stable E_T of 2.38 ± 0.03 eV.

The excited state lifetimes of the complexes were also recorded in 2-MeTHF solution. The average excited state lifetimes (τ_{avg}) of these complexes, ranging from a few nanoseconds (ns) to a few tens of microseconds (µs) could be fitted with either mono- (complexes **1**, **2**, **4**, and **13**-**15**) or bi-exponential (complexes **3**, **5**-**9**, **11**, **12** and **16**) decay models, respectively (Table S2 in the Supporting Information). In addition, the excited state lifetime traces of complex **5** were resolved with respect to each PL emission peaks at 298 and 77 K (Table S3 in the Supporting Information). This complex exhibits a bi-exponential decay profile. At 298 K and PL emission maxima of 561 nm, complex **5** displays both a prompt component with a lifetime τ_1 of 3.82 ns, and a delayed component with a lifetime τ_2 of 517.9 ns. Moreover, at 77 K, the first emission peak of 486 nm shows an average excited state lifetime of 3.49 ns, which could be attributed to fluorescence emission due to charge transfer. The second emission peak at 520 nm exhibits the τ_{avg} of 788 ns, with a prompt (τ_1 = 3.85 ns) and a delayed component (τ_2 = 8224 ns) as well. Long delayed emission components in this complex can be attributed to dual emission due to closely lying ^{3}IL and ^{3}LLCT excited states. In addition, a very strong PL quenching in the non-degassed gold(III) complex solutions was also observed due to the presence of oxygen, which further supports the idea of the emission profile being dominated by phosphorescence transitions.[28]

10.1002/chem.202003571

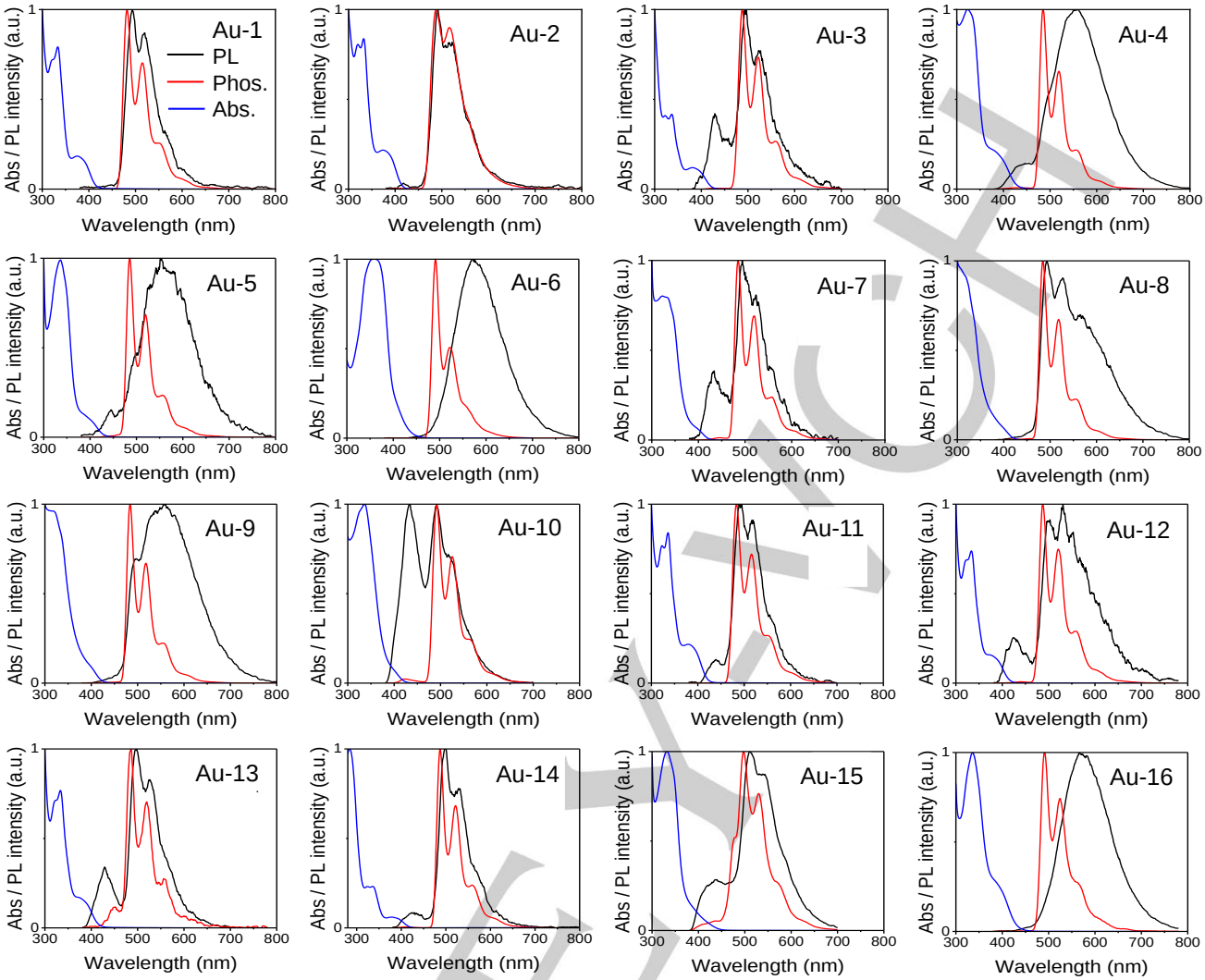

Figure 1. Absorbance (Abs) in blue (in THF at 298 K), photoluminescence (PL) spectra in black (in CH_2Cl_2 at 298 K) and phosphorescence (Phos.) spectra in red (in 2-MeTHF at 77 K) of **1**-**16**.

Electrochemical properties. The cyclic voltammetry of complexes **1**-**5** and **7**-**16** was measured using a glassy carbon-electrode and a platinum (Pt) wire counter electrode in dichloromethane solutions (See Figure S1 in the Supporting Information). The highest occupied molecular orbital (HOMO) energy levels were extracted using oxidation potential values. The lowest unoccupied molecular orbital (LUMO) energy levels were estimated through substitution of the E_g with the HOMO energy levels. Complexes **1**-**3** and **8**-**14** show irreversible oxidation potential ranging between 0.50 and 1.09 eV. On the other hand, complexes **4**-**7**, **15** and **16** exhibit either quasi-reversible or reversible oxidation potentials, which vary between 0.36 and 0.76 eV. The energy levels of the HOMO and LUMO of all gold(III) complexes were also calculated and summarized in Table S2 in the Supporting Information.

Computational studies. DFT and TDDFT calculations were carried out to gain a deeper understanding of the electronic structures and the origin of the electronic transitions in these systems.

The optimized ground-state (S_0) geometries of complexes **1**-**16** with selected structural parameters are shown in the Supporting Information (Figure S7 in the Supporting Information). Complexes bearing an alkynyl group bound to the gold atom (**4**-**6**, **7** and **14**-**16**) displayed a Au-C_3 distance of 2.04 Å, which is very similar to that found in complex **2** for the Au-F bond (2.02 Å). When the gold center is directly connected to a Csp^2 atom (**11**) or a carbene moiety (**12**), the distance increased to 2.10 Å. The Au-Cl bond (2.41 Å) in **1** is the longest among all the complexes described here. It is noteworthy that the trend observed in the distances calculated for **1** and **2** can be correlated with the experimental values measured in the crystal structures determined by X-ray diffraction analysis of similar complexes (2.37 and 2.05 Å, respectively, see Supporting Information).[18a-b] The distances and the angles of the κ^3-(N^C^C) pincer are not affected when the substitution patterns were modified. As expected, complex **3**

adopts an almost coplanar geometry between the ancillary ligand and the pincer with an angle of 11.5°, while in **11** this angle increased to 61° as a result of the steric repulsion between the hydrogen atoms on the aryl ancillary ligand and the ones on the κ^3-(N^C^C) pincer template, which is in good correlation with the experimental value of 55.58° measured in the crystal structure of an analogous 4-^{t}Bu-aryl derivative **11'** (See Supporting Information)[18b]. In a similar manner, the NHC ligand in **12** is placed in a pseudo orthogonal disposition to the plane of the pincer template. The introduction of carbazole or fluorene moieties onto the ancillary ligand tends to break the coplanarity between these two moieties as seen for complexes **5** and **6**. However, replacing the phenyl group in **5** by a pyridine ring in **7** restored the coplanarity, likely as a result of the enhanced electronic delocalization within the electron-deficient heteroaromatic moiety.

Moreover, changing the *tert*-butyl groups on the pincer ligand by mesityl (**14**) or by methoxy groups (**15**) as well as replacing one carbazole moiety with another κ^3-(N^C^C)Au(III) group in **16** re-established the coplanarity between the ancillary ligand and the pincer scaffold.

The first ten singlet-singlet transitions of **1**-**16** and the frontier orbitals involved were calculated by the TDDFT/CPCM method (see Table S5 and Figures S8 to S23 in the Supporting Information). The computed $S_0 \rightarrow S_1$ transitions are in line with the trend in the absorption wavelength determined experimentally: **1** and **2** (367)<**14** (372)≈**11** (373)<**3** and **12** (378)<**7** (402)<**4** and **5** (438)<**15** (436)<**16** (446)<**6** (459). An important red-shift can be seen by tuning the nature of the ancillary ligand from electron-deficient (**1**-**3**, **11**, **14**) to electron-rich (**4**-**7, 15**, **16**). Taking a closer look at the transitions with significant oscillator strengths for the low-lying absorption bands, we can note three major contributions for complexes **1** and **2** stemming from the $HOMO_{NCC} \rightarrow LUMO_{NCC}$, $HOMO\text{-}1_{NCC} \rightarrow LUMO_{NCC}$ and $HOMO\text{-}1_{NCC} \rightarrow LUMO+1_{NCC}$ excitations, displaying only IL [$\pi_{NCC} \rightarrow \pi^*_{NCC}$] transitions. Moving to the electron-deficient alkynyl derivative **3**, in addition to the IL [$\pi_{NCC} \rightarrow \pi^*_{NCC}$], LLCT [$\pi_{alkynyl} \rightarrow \pi^*_{NCC}$] transitions appear as a result of $HOMO\text{-}1_{alkynyl} \rightarrow LUMO_{NCC}$ excitations. The same type of transitions can be observed when the *tert*-butyl groups are replaced by mesityl rings on the pincer template (**14**). When electron-donating *N*-aryl-alkynyl groups are introduced (**4**-**6**), the HOMO orbital is mostly localized on the ancillary ligand, rendering the $HOMO_{ancillary} \rightarrow LUMO_{NCC}$ contribution as the most relevant LLCT transition. More contributions can be found for those complexes which exhibit IL [$\pi_{ancillary} \rightarrow \pi^*_{ancillary}$] transitions as well. As previously described, the modifications on the pincer ligand (**15**) or the introduction of an heteroaryl in the alkynyl ligand (**7**) do not change the nature of the transitions compared to the parent complex (**5**). When the ancillary ligand features an electron deficient aryl or a strong σ-donor NHC directly connected to the gold atom, the $HOMO_{NCC} \rightarrow LUMO_{NCC}$, $HOMO\text{-}1_{NCC} \rightarrow LUMO_{NCC}$ and $HOMO\text{-}1_{NCC} \rightarrow LUMO+1_{NCC}$ transitions become most relevant so that, as in the case of complexes **1**-**3**, IL[$\pi_{NCC} \rightarrow \pi^*_{NCC}$] play a predominant role. Finally, for the binuclear complex **16**, the major contributions stem from the $HOMO_{ancillary} \rightarrow LUMO_{NCC}$ (LLCT) and the $HOMO\text{-}2_{NCC} \rightarrow LUMO_{NCC}$ and the $HOMO\text{-}3_{NCC} \rightarrow LUMO+1_{NCC}$ (IL) excitations, thus resulting in a combination of LLCT and IL transitions. Overall, these results clearly illustrate the significant effect that the alkynyl moiety imparts to the population of the different frontier molecular orbitals within these complexes and thus, how the localization of the HOMO onto the ancillary ligand fosters the contributions of the LLCT [$\pi_{ancillary} \rightarrow \pi^*_{NCC}$] transitions to the overall absorption spectra.

Geometry calculations of the lowest-lying triplet excited states (T_1) were performed with the unrestricted UPBE0 method to provide further insights into the nature of the emissive states of complexes **1**-**16** and the structural changes from their corresponding ground states. Differences in bond lengths between the T_1 states and the corresponding ground states S_0 of **1**-**16** are shown in Figure S24. No major geometrical changes were found for those complexes, retaining the geometry in both their S_0 and T_1 states and displaying almost no excited state structure distortion.

The plots of the spin density of their emissive states can be found in Figure S25. The spin density in complexes **1**-**3**, **10**-**12** and **14** is mainly localized on the κ^3-(N^C^C) pincer and the metal center, which supports the ^{3}IL character of the observed transitions with some perturbations from the metal center of their T_1 states. For complexes **4**-**7**, **15** and **16**, the spin density is mainly localized on both the pincer and the ancillary ligand as well as on the metal center, supporting a mixture of metal-perturbed ^{3}IL and ^{3}LLCT transitions for **4**-**6** and a ^{3}LLCT character for **7**, **15** and **16** in their T_1 state.

The calculated emission energies of complexes **1**-**16** are listed in Table S6. They result from the approximation of the energy difference between the S_0 and T_1 states at their corresponding optimized geometries in THF. Interestingly, despite differences in the absolute values, the trends resulting from the calculated emission energies successfully mimic those observed in the experimental spectra. The computed emission wavelengths for **3** (478), **11** (474), **12** (479) and **14** (473) are slightly red shifted compared to those calculated for **7** (463), **1** (469) and **2** (470). For complexes **4** and **5** (500), **6** (522), **16** (509) and **15** (497), a much higher red shift is predicted, which can justify the observed yellowish-green emission. As expected, replacing electron-withdrawing alkynyl group in **3** with an electron-donating one (**4**, **5** and **15**) resulted in a significant red-shift of ≥ 20 nm, as a result of a destabilized HOMO orbital and thus a narrower HOMO-LUMO energy gap (see the computed orbital energy diagrams of the frontier molecular orbitals in Figure S26 in the Supporting Information). This red shift increased to ca. 45 nm when fluorene groups are introduced in the ancillary ligand (**6**), as already observed by Yam and coworkers in other gold systems.[12e] The important red shift observed with the introduction of a second κ^3-(N^C^C)Au(III) pincer (**16**) can be explained as a result of the strengthened π-conjugation between donor and acceptor pairs that stabilize the LUMO of the pincer ligand. Further, the increase of the π-stacking between the molecules due to a more planar structure compared to the homologue **5** might also help to explain the observed shift (see Figure S7).[12d,17a]

OLED device fabrication. The EL of complexes **1**-**16** was evaluated in solution-processed OLED devices with a typical layer sequence of indium tin oxide (ITO) anode / hole transporting layer (HTL) / emissive layer (EML = gold(III) complexes + host) / electron transporting layer (ETL) / electron injection layer (EIL) / aluminum (Al) cathode (see section 8 in the Supporting Information). The optimization of several criteria such as the type of host material, the doping concentration of emitter, the thickness of both HTL and ETL was carried out using complexes **5** and **7** as benchmark dopants.

First, an appropriate host matrix was carefully screened from a series of molecular and polymeric materials including 4,4'-bis-(*N*-carbazolyl)-1,1'-biphenyl (CBP), bis-4-(*N*-carbazolyl)-phenyl)-

10.1002/chem.202003571

phenylphosphine oxide (BCPO), 2,6-bis-(3-(9*H*-carbazol-9-yl)phenyl)pyridine (26DCzPPy), poly(9-vinylcarbazole) (PVK) and mixed PVK : 1,3-bis[2-(4-tert-butylphenyl)-1,3,4-oxadiazo-5-yl]benzene (OXD-7; 60:40) hosts by doping the EML (30 ± 5 nm) with 5 to 20 wt% of complexes **5** and **7** in the CH_2Cl_2 solution (see section 8 in the Supporting Information). These EMLs were deposited between the HTL (~33 nm) and ETL (35 nm). Table 1 summarizes the effect of host materials on the EL characteristics of the devices based on complexes **5** and **7**. The EL spectra of **5**-based devices display a strong dependence on the host material resulting in a peak emission ranging from 496 to 528 nm when the latter is changed from BCPO to PVK. In contrast, a stable peak EL emission at 500 nm can be observed for **7** even by changing the host from CBP to 26DCzPPy as shown in Figure 4. The device based on complex **5** in CBP shows a maximum current efficiency (η_{CE}) of 7.91 cd.A^{-1} and an external quantum efficiency (η_{ext}) of 2.62%. The resulting η_{CE} (η_{ext}) increased from 4.53 cd.A^{-1} (1.43%) to 11.48 cd.A^{-1} (3.68%) when the host was changed from a polymeric hole transporting PVK to a bipolar 26DCzPPy hosts (Table 1). We attributed this improvement to the balance carrier injection and higher E_T of the 26DCzPPy.[29] The device performance could be further improved to 15.19 cd.A^{-1} (5.1%) by blending the *p*-type PVK with *n*-type OXD-7[30] hosts in an optimal ratio of 60:40. The PVK:OXD-7 blend is suitable for spin-casted host because of their excellent solubility in common organic solvents, their bipolar carrier transporting characteristics, high E_T (preventing the back energy transfer) and smooth thin-film morphologies.[29a,31] The η_{CE} and η_{ext} were greatly improved to 25.6 cd.A^{-1} and 8.3% respectively, when the doping concentration of **5** is reduced from 10 to 5 wt% in the PVK:OXD-7 mixed host matrix (Table S4). The improved performance can be attributed to substantial suppression in the concentration quenching of **5**.[32] Moreover, the device also shows a 4 nm blue-shift in the EL spectra, which is peaking at 524 nm (Figure 5a). Eventually, the η_{CE} and η_{ext} of the devices further increased to 30.26 cd.A^{-1} and 9.82% when the EML was prepared in toluene solution and the ETL (TPBi) thickness was increased from 35 to 45 nm (Table 2). Similarly, **7** was employed as an emitter in the optimized device architecture, which is ITO (120 nm) / PEDOT:PSS (35 nm) / EML (**7** + host) (40 nm) / TPBi (45 nm) / LiF (1 nm) / Al (100 nm), with the four best host materials that were utilized for the devices fabricated with complex **5**. The doping concentration of **7** was varied from 5 to 20 wt% in the host matrices. Upon increasing the concentration of **7** in the PVK:OXD-7 (60:40) host matrix from 5 to 20 wt%, a stable sky-blue emission is observed at 500 nm (Figure 5b). Interestingly, the emission maxima remained intact at 500 nm with all hosts, including CBP, PVK, 26DCzPPy, and PVK:OXD-7 (60:40), when the dopant concentration varied from 5 to 20 wt%. However, a feeble host emission has been observed in the CBP and 26DCzPPy hosts-based devices, particularly at low dopant concentrations (Figure S2). The best device efficiencies were observed for a doping of 15 wt% of **7** in CBP, BCPO and 26DCzPPy hosts, except in PVK:OXD-7 blend, which discloses a higher performance for 10 wt% emitter-doped EML. The devices show an ascending η_{CE} and η_{ext} values from 15.14 to 29.87 cd.A^{-1} and 4.93 to 9.51% when the host material was changed from CBP < BCPO < 26DCzPPy < PVK:OXD-7, as summarized in Table 1. The high performance in the PVK:OXD-7 (60:40) host is attributed to the good film forming properties of PVK:OXD-7 blend and the ability of OXD-7 to suppress the electron trapping.[33] Moreover, upon doping a 15 wt% of complex **7** in the mixed PVK:OXD-7 (60:40) host matrix, the resulting thin film emissive layer showed a highest η_{PL} of 30.5%, which is significantly higher than that obtained with CBP (14 ± 1%), BCPO (15 ± 1.2%), and 26DCzPPy (18 ± 0.5%) host-based emissive layers. The substantial variation in the solid-state η_{PL} could be attributed to three major factors: (i) polarity of host that influences the contribution of radiative excited states, (ii) host-to-guest energy transfer, and (iii) minimization of self-aggregation within the emitter molecules. Complex **7**-based device performance of η_{PL} of 30.5% represents a ca. 17% increase with respect to that obtained for complex **5**.

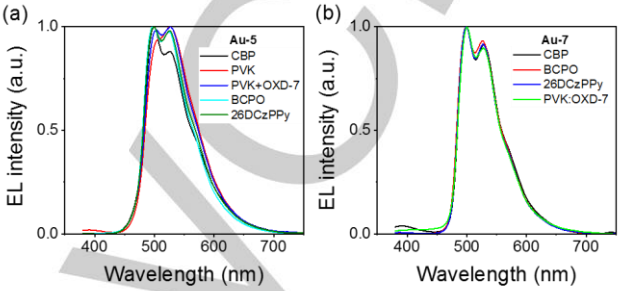

Figure 4. Effect of host materials, such as CBP, PVK, BCPO, 26DCzPPy, PVK:OXD-7, on the EL spectra of **5** and **7** complexes.

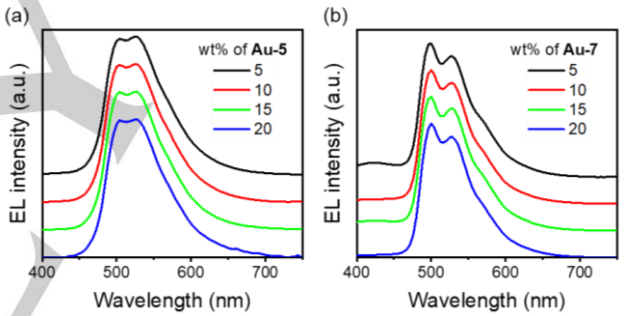

Figure 5. EL spectra of OLED devices by varying the emitters, **5** and **7,** doping concentrations from 5 to 20 wt% in the PVK:OXD-7 (60:40) mixed ambipolar host matrix.

Table 1. Effect of different host materials on the EL characteristics of complex **5** and **7** containing solution-processed OLED devices.

Complex	Host	λ_{EL} (nm)	η_{CE} (cd.A^{-1})	η_{PE} (lm.W^{-1})	η_{ext} (%)
5	PVK	528	4.53	2.37	1.43
	CBP	500	7.91	2.97	2.62
	BCPO	496	10.24	4.29	3.34
	26DCzPPy	524	11.48	5.15	3.68
	PVK:OXD-7	528	15.19	10.61	4.93
7	CBP	500	15.4	8.06	4.93
	BCPO	500	17.2	9.03	5.47
	26DCzPPY	500	26.2	16.5	8.28
	PVK:OXD-7	500	29.9	20.9	9.51

10.1002/chem.202003571

Next, all gold(III) complexes were tested in the optimized device architecture, with their EMLs prepared in CH_2Cl_2, as their solubility was limited in toluene. Table 2 summarizes the EL characteristics of **1**-**16** in the PVK:OXD-7 (60:40) blend host matrix. The peak EL emission of **1**-**16** ranges between sky-blue (496 nm) to yellowish-green (544 nm) (Figure S3 in the Supporting Information). The device performance of complexes **1**-**15** is presented in Figures S4-S6. Replacing the halogen atoms (**1** and **2**) by an electron-deficient alkynyl ligand (**3**) leads to a bathochromic shift in the EL emission (λ_{EL}) of 32 nm and a bluish-green emission with $CIE_{x,y}$ of (0.250,0.489). The current, power and external efficiencies (η_{CE}, η_{PE} and η_{ext}) decrease significantly compared to **1**, with values of 2.31 cd.A^{-1}, 1.33 lm.W^{-1} and 1.07%, respectively (Figure S4). Tuning the electronic properties of the alkynyl ligand using the electron-donating aminophenylalkynyl moiety (**4**-**6**) barely modifies the λ_{EL} and the $CIE_{x,y}$. However, the η_{CE}, η_{PE} and η_{ext} are significantly increased, reaching a maximum of η_{CE} of 46.6 cd.A^{-1} and η_{ext} of 14% for **6**-based device, which is the highest among all the complexes studied herein, due to the high η_{PL} of 26.3%. (Table 2). The substitution of the phenyl ring (**6**) by a pyridine (**7**) leads to a hypsochromic shift of 32 nm in the λ_{EL} and a slight blue shift in the color of emission with $CIE_{x,y}$ of (0.260,0.578). The introduction of aryl or NHC ligands did not bring any significant improvement. However, the modifications on the κ^3-(N^C^C) pincer were more noticeable. Indeed, the introduction of mesityl groups (**14**) resulted in a hypsochromic shift of 24 nm, a significant increase regarding the η_{CE}, η_{PE} and η_{ext} but most importantly, in an intense green emission with $CIE_{x,y}$ of (0.271,0.608) with respect to **3**. In contrast, the introduction of methoxy groups in **15** led to a bathochromic shift, a decrease of η_{CE}, η_{PE} and η_{ext} and a yellowish-green emission with $CIE_{(x,y)}$ of (0.328,0.594), with respect to **5**. Concerning the first binuclear gold(III)-based device (**16**), the EL characteristics are very similar to those of complex **5** and comparable with those of OLEDs based on binuclear heavy metals.[34] Our best device, based on mononuclear complex **6**, shows an 8 nm red-shifted emission maxima at 532 nm and almost 3 folds higher η_{CE} and 2.6 folds higher η_{ext} compared to the binuclear complex **16** (Figure 6).

Table 2. Effect of gold(III) complexes on the electroluminescence characteristics of solution-processed OLED devices. 10 wt% was used for all complexes in the mixed host system, except complex **5**, which was doped with 5 wt%.

Complex	λ_{EL} (nm)	η_{CE} (cd.A^{-1})	η_{PE} (lm.W^{-1})	η_{ext} (%)	$CIE_{(x,y)}$
1	496	11.56	7.26	3.74	(0.265,0.563)
2	496	3.49	1.29	1.24	(0.270,0.513)
3	528	2.31	1.33	1.07	(0.250,0489)
4	528	18.15	12.7	4.27	(0.306,0.571)
5	524	30.26	19.01	9.82	(0.267,0.554)
6	532	46.6	32.6	14.0	(0.329,0.577)
7	500	29.87	20.85	9.51	0.260,0.578)
8	532 544	2.30	1.45	0.70	(0.331,0.586)
9	504 532	4.47	2.81	1.39	(0.286,0.585)
10	500	6.55	4.12	2.07	(0.269,0.577)
11	496	3.99	2.78	1.28	(0.246,0.583)
12	504	0.06	0.03	0.02	(0.276,0.581)
13	496 500	6.04	4.74	2.11	(0.246,0.518)
14	504	6.89	4.81	2.17	(0.271,0.608)
15	520 540	25.89	18.1	7.57	(0.328,0.594)
16	524	16.00	14.40	5.36	(0.280,0.565)

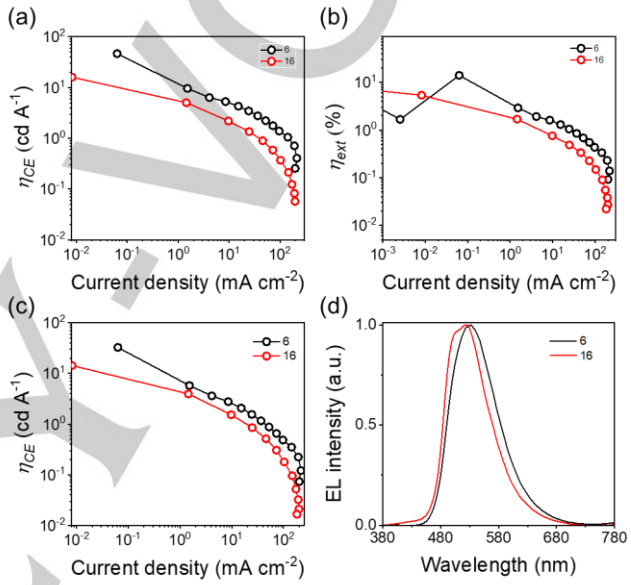

Figure 6. EL characteristics of devices consisting 10 wt% of complex **6** and **16** in the PVK:OXD-7 (60:40) host.

Conclusion

In summary, a comprehensive study of the photophysical properties of novel bis-cyclometalated gold(III) complexes stabilized by a κ^3-(N^C^C) pincer scaffold is presented here. These complexes could be accessed easily via ligand exchange or transmetalation reactions from the corresponding gold(III)-halides. Most of the studied compounds displayed strong absorbance in the ultraviolet region ranging from 300 to 390 nm and a low absorption band from 400 to 460 nm. The shape and the range of the PL spectra significantly vary within the series (424 to 572 nm) as a result of the different contributions of ^{3}LLCT [$\pi_{ancillary} \rightarrow \pi^*_{NCC}$] and the metal perturbed ^{3}IL [$\pi \rightarrow \pi^*$] transitions reflecting the impact that structural modifications in both ancillary and pincer ligands have on the emissive properties of these species. DFT and TDDFT calculations provided further analysis on the nature of the transitions involved and showcased the significant effect of the alkynyl moiety on the population of the different frontier molecular orbitals. The complexes have been applied to solution-processable OLEDs with peak EL emission ranging between sky-blue (496 nm) to yellowish-green (544 nm). The best material has been obtained with (bis-fluorene)aminophenylalkyne as the ancillary ligand (**6**), displaying

η_{CE} of 46.6 cd.A^{-1}, η_{PE} of 32.6 lm.W^{-1} and η_{ext} of 14%. Promising results could also be obtained with (bis-carbazole)aminophenylalkynyl (**5**) and (bis-carbazole)aminopyridinealkynyl (**7**) as ancillary ligands, with η_{ext} of 9.82 and 9.51% respectively. Moreover, we also presented the first example of an efficient green device based on a binuclear gold(III) complex. The described performances confirm the promising potential of the κ^3-(N^C^C) template to develop a new class of efficient light emitting materials.

Experimental Section

The following information can be found in the Supporting Information of this manuscript: synthetic routes and characterization of complexes **1**-**16**. Photophysical properties. Cyclic voltammetry. Materials used in the preparation of OLED. OLED device fabrication and characterization. DFT calculations.

Acknowledgements

CN thank the European Research Council (ERC Starting grant agreement no. 307948) and the Swiss National Science Foundation (SNF) (200020-146853), for financial support. CJS is grateful for the financial support from SNF (200021-178944) and ETH Zurich.

Keywords: gold(III) • κ^3-(N^C^C) • OLED • emitter • phosphorescent

[1] M. Pope, H. P. Kallmann, *J. Chem. Phys.* **1963**, *38*, 2042-2043.

[2] C. W. Tang, S. A. VanSlyke, *Appl. Phys. Lett.* **1987**, *51*, 913.

[3] P. K. Bhatnagar, *Khan Z. (eds) Nanomaterials and Their Applications. Advanced Structured Materials* **2018**, *84*, 261-287.

[4] M. A. Baldo, M. E. Thompson, S. R. Forrest, *Nature* **2000**, *403*, 750-753.

[5] M. Kleinschmidt, C. van Wüllen, C. M. Marian, *J. Chem. Phys.* **2015**, *142*, 094301.

[6] a) M. A. Baldo, D. F. O'Brien, M. E. Thompson, S. R. Forrest, *Phys. Rev. B.* **1999**, *60*, 14422-14428; b) H. Yersin, A. F. Rausch, R. Czerwieniec, T. Hofbeck, T. Fischer, *Coord. Chem. Rev.* **2011**, *255*, 2622-2652

[7] a) C. Adachi, M. A. Baldo, M. E. Thompson, S. R. Forrest, *J. Appl. Phys.* **2001**, *90*, 5048-5051; b) S. Lamansky, P. Djurovich, D. Murphy, F. Abdel-Razzaq, H.-E. Lee, C. Adachi, P. E. Burrows, S. R. Forrest, M. E. Thompson, *J. Am. Chem. Soc.* **2001**, *123*, 4304-4312; c) B. W. D'Andrade, M. E. Thompson, S. R. Forrest, *Adv. Mater.* **2002**, *14*, 147-151; d) X. Ren, J. Li, R. J. Holmes, P. I. Djurovich, S. R. Forrest, M. E. Thompson, *Chem. Mater.* **2004**, *16*, 4743-4747; d) Y. Kawamura, K. Goushi, J. Brooks, J. J. Brown, H. Sasabe, C. Adachi, *Appl. Phys. Lett.* **2005**, *86*, 071104; f) H. J. Bolink, E. Coronado, S. G. Santamaria, M. Sessolo, N. Evans, C. Klein, E. Baranoff, K. Kalyanasundaram, M. Graetzel, M. K. Nazeeruddin, *Chem. Commun.* **2007**, 3276-3278; g) H. Fu, Y.-M. Cheng, P.-T. Chou, Y. Chi, *Mater. Today* **2011**, *14*, 472-479; h) P.-N. Lai, C. H. Brysacz, M. K. Alam, N. A. Ayoub, T. G. Gray, J. Bao, T. S. Teets, *J. Am. Chem. Soc.* **2018**, *140*, 10198-10207.

[8] a) M. A. Baldo, D. F. O'Brien, Y. You, A. Shoustikov, S. Sibley, M. E. Thompson, S. R. Forrest, *Nature* **1998**, *395*, 151-154; b) M. Hissler, J. E. McGarrah, W. B. Connick, D. K. Geiger, S. D. Cummings, R. Eisenberg, *Coord. Chem. Rev.* **2000**, *208*, 115-137; c) D. R. McMillin, J. J. Moore, *Coord. Chem. Rev.* **2002**, *229*, 113-121; d) W. Lu, B.-X. Mi, M. C. Chan, Z. Hui, C.-M. Che, N. Zhu, S.-T. Lee, *J. Am. Chem. Soc.* **2004**, *126*, 4958-4971; e) F. N. Castellano, I. E. Pomestchenko, E. Shikhova, F. Hua, M. L. Muro, N. Rajapakse, *Coord. Chem. Rev.* **2006**, *250*, 1819-1828; f) C. Lee, R. Zaen, K.-M. Park, K. H. Lee, J. Y. Lee, Y. Kang, *Organometallics* **2018**, *37*, 4639-4647.

[9] a) H. Rudmann, S. Shimada, M. F. Rubner, *J. Am. Chem. Soc.* **2002**, *124*, 4918-4921; b) S. Welter, K. Brunner, J. W. Hofstraat, L. De Cola, *Nature* **2003**, *421*, 54-57; c) Y.-L. Tung, P.-C. Wu, C.-S. Liu, Y. Chi, J.-K. Yu, Y.-H. Hu, P.-T. Chou, S.-M. Peng, G.-H. Lee, Y. Tao, A. J. Carty, C.-F. Shu, F.-L. Wu, *Organometallics* **2004**, *23*, 3745-3748; d) P.-T. Chou, Y. Chi, *Chem. Soc. Rev.* **2007**, *36*, 1421-1431; e) B.-S. Du, J.-J. Liao, M.-H. Huang, C.-H. Lin, H.-W. Lin, Y. Chi, H.-A. Pan, G.-L Fan, K.-T. Wong, G.-H. Lee, P.-T. Chou, *Adv. Funct. Mater.* **2012**, *22*, 3491-3499. f) W.-K. Chu, S.-M. Yiu, C.-C. Ko, *Organometallics* **2014**, *33*, 6771-6777.

[10] J. K. Borchardt, *Mater. Today* **2004**, *7*, 42-46.

[11] Y. Cao, I. D. Parker, G. Yu, C. Zhang, A. J. Heeger, *Nature* **1999**, *397*, 414-417.

[12] A. Vogler, H. Kunkely, *Coord. Chem. Rev.* **2001**, *219-221*, 489-507; b) V. W.-W. Yam, E. C.-C. Cheng, *Chem. Soc. Rev.* **2008**, *37*, 1806-1813; c) R. Kumar, C. Nevado, *Angew. Chem. Int. Ed.* **2017**, *56*, 1994-2015; d) C.-H. Lee, M.-C. Tang, Y.-C. Wong, M.-Y. Chan, V. W. W. Yam, *J. Am. Chem. Soc.* **2017**,*139*, 10539-10550; e) M.-C. Tang, C.-H. Lee, M. Ng, Y.-C. Wong, V. W.-W. Yam, *Angew. Chem. Int. Ed.* **2018**, *57*, 5463-5466.

[13] a) P.-K. Chow, C. Ma, W.-P. To, G. S. Ming Tong, S.-L. Lai, S. C. F. Kui, W.-M. Kwok, C.-M. Che, *Angew. Chem. Int. Ed.* **2013**, *52*, 11775-11779. b) P.-K. Chow, G. Cheng, G.G. S. Ming Tong, C. Ma, W.-M. Kwok, W.-H. Ang, C. Y.-S. Chung, C. Yang, F. Wang, C.-M. Che, *Chem. Sci.* **2016**, *7*, 6083-6098.

[14] (a) M. Hashimoto, S. Igawa, M. Yashima, I. Kawata, M. Hoshino, M. Osawa, *J. Am. Chem. Soc.* **2011**, *133*, 10348-10351. b) R. Hamze, L. L. Peltier, D. Sylvinson, M. Jung, J. Cardenas, R. Haiges, M. Soleilhavoup, R. Jazzar, P. I. Djurovich, G. Bertrand, M. E. Thompson, *Science* **2019**, *363*, 601-606.

[15] a) W. J. Wolf, M.S. Winston, F. D. Toste, *Nature Chem.* **2014**, *6*, 159-164. b) J. Gil-Rubio, J. Vicente, *Dalton Trans.* **2015**, *44*, 19432-19442. c) H. Kawai, W. J. Wolf, A. G. DiPasquale, M. S. Winston, F. D. Toste, *J. Am. Chem. Soc.* **2016**, *138*, 587-593

[16] a) V. W.-W. Yam, K. M.-C. Wong, L.-L. Hung, N. Zhu, *Angew. Chem. Int. Ed.* **2005**, *44*, 3107-3110; b) W.-P. To, G. S.-M. Tong, W. Lu, C. Ma, J. Liu, A. L.-F. Chow, C.-M. Che, *Angew. Chem. Int. Ed.* **2012**, *51*, 2654-2657; c) W.-P. To, D. Zhou, G. S. M. Tong, G. Cheng, C. Yang, C.-M. Che, *Angew. Chem. Int. Ed.* **2017**, *56*, 14036-14041.

[17] a) V. K.-M. Au, K. M.-C. Wong, D. P.-K. Tsang, M.-Y. Chang, N. Zhu, V. W.-W. Yam, *J. Am. Chem. Soc.* **2010**, *132*, 14273-14278; b) M.-C. Tang, D. P.-K. Tsang, M. M.-Y. Chen, K. M.-C. Wong, V. W.-W. Yam, *Angew. Chem. Int. Ed.* **2013**, *52*, 446-449; c) W.-P. To, K. T. Chan, G. S. M. Tong, C. Ma, W.-M. Kwok, X. Guan, K.-H. Low, C.-M. Che, *Angew. Chem. Int. Ed.* **2013**, *52*, 6648-6652; d) M.-C. Tang, C. K.-M. Chan, D. P.-K. Tsang, Y.-C. Wong, M. M.-Y. Chan, K. M.-C. Wong, V. W.-W. Yam, *Chem. Eur. J.* **2014**, *20*, 15233-15241; e) M.-C. Tang, D. P.-K. Tsang, Y.-C. Wong, M.-Y. Chan, K. M.-C. Wong, V. W.-W. Yam, *J. Am. Chem. Soc.* **2014**, *136*, 17861-17868; f) G. Cheng, K. T. Chan, W.-P. To, C.-M. Che, *Adv. Mater.* **2014**, *26*, 2540-2546; g) M.-C. Tang, C.-H. Lee, S.-L. Lai, M. Ng, M.-Y. Chan, V. W.-W Yam, *J. Am. Chem. Soc.* **2017**, *139*, 9341-9349; h) C.-H. Lee, M.-C. Tang, W.-L. Cheung, S.-L. Lai, M.-Y. Chan, V. W.-W. Yam, *Chem. Sci.* **2018**, *9*, 6228-6232.

[18] a) R. Kumar, A. Linden, C. Nevado, *Angew. Chem. Int. Ed.* **2015**, *54*, 14287-14290; b) R. Kumar, A. Linden, C. Nevado *J. Am. Chem. Soc.* **2016**, *138*, 13790; c) R. Kumar, J.-P. Krieger, E. Gómez-Bengoa, T. Fox, A. Linden, C. Nevado, *Angew. Chem. Int. Ed.* **2017**, *56*, 12862-12865; d) H. Beucher, E. Merino, A. Genoux, T. Fox, C. Nevado, *Angew. Chem. Int. Ed.* **2019**, *58*, 9064-9067.

[19] L.-K. Li, M.-C. Tang, S.-L. Lai, M. Ng, W.-K. Kwok, M.-Y. Chan, V. W.-W. Yam, *Nature Photon.* **2019**, *13*, 185-191.

[20] W.-K. Kwok, M.-C. Tang, S.-L. Lai, W.-L. Cheung, L.-K. Li, M. Ng, M.-Y. Chan, V. W.-W. Yam, *Angew. Chem. Int. Ed.* **2020**, *59*, 10.1002/anie.202001972.

[21] H. Beucher, S. Kumar, E. Merino, W.-H. Hu, G. Stemmler, S. Cuesta-Galisteo, J. A. González, J. Jagielski, C.-J. Shih, C. Nevado, *Chem. Mater.* **2020**, *32*, 1605-1611.

[22] W.-Y. Wong, C.-L. Ho, *Coord. Chem. Rev.* **2009**, *253*, 1709-1758.

[23] Y. Im, M. Kim, Y. J. Cho, J.-A. Seo, K. S. Yook, J. Y. Lee, *Chem. Mater.* **2017**, *29*, 1946-1963.

[24] a) J. Vicente, M.-T. Chicote, M. M. Alvarze-Falcón, *Organometallics* **2005**, *24*, 5956-5963; b) A. Gutiérrez-Blanco, V. Fernández-Moreira, M. C. Gimeno, E. Peris, M. Poyatos, *Organometallics* **2018**, *37*, 1795-1800.

[25] a) K.-C. Yim, V. K.-M. Au, L.-L. Hung, K. M.-C. Wong, V. W.-W. Yam, *Chem. Eur. J.* **2016**, *22*, 16258-16270; b) K.-C. Yim, V. K.-M. Au, K. M.-C. Wong, V. W.-W. Yam, *Chem. Eur. J.* **2017**, *23*, 5772-5786.

[26] For further information, see Supporting Information.

[27] a) V. W.-W. Yam, K. H.-Y. Chan, K. M.-C. Wong, N. Zhu, *Chem. Eur. J.* **2005**, *11*, 4535-4543; b) D. I. Wozniak, W. A. Sabbers, K. C. Weerasiri, L. V. Dinh, J. L. Quenzer, A. J. Hicks, G. E. Dobereiner, *Organometallics* **2018**, *37*, 2376-2385.

[28] a) M. A. Filatov, S. Baluschev, K. Landfester, *Chem. Soc. Rev.* **2016**, *45*, 4668-4689; b) Y.-L. Chen, S.-W. Li, Y. Chih, Y.-M. Chen, S.-C. Pu, Y.-S. Yeh, P.-T. Chou, *ChemPhysChem* **2005**, *6*, 2012-2017.

[29] J.-H. Jou, S. Kumar, P.-H. Fang, A. Venkateswararao, K. R. J. Thomas, J.-J Shyue, Y.-C. Wang, T.-H. Li, H.-H. Yu, *J. Mater. Chem. C* **2015**, *3*, 2182-2194; b) J.-H. Jou, W.-B. Wang, S.-M. Shen, S. Kumar, I. M. Lai, J.-J. Shyue, S. Lengvinaite, R. Zostautiene, J. V. Grazulevicius, S. Grigalevicius, S.-Z. Chen, C.-C. Wu, *J. Mater. Chem.* **2011**, *21*, 9546-9552.

[30] a) J. Lee, N. Chopra, S.-H. Eom, Y. Zheng, J. Xue, F. So, J. Shi, *Applied Physics Letters* **2008**, *93*, 123306; b) T. Ye, S. Shao, J. Chen, L. Wang, D. Ma, *ACS Applied Materials & Interfaces* **2011**, *3*, 410-416.

[31] K. S. Yook, J. Y. Lee, *Advanced Materials* **2014**, *26*, 4218-4233.

[32] a) Y.-Z. Shi, K. Wang, X. Li, G.-L. Dai, W. Liu, K. Ke, M. Zhang, S.-L. Tao, C.-J. Zheng, X.-M. Ou, X.-H. Zhang, *Angew. Chem. Int. Ed.* **2018**, *57*, 9480-9484; b) C. Murawski, K. Leo, M. C. Gather, *Adv. Mater.* **2013**, 25, 6801-6827.

[33] a) S. Wang, B. Zhang, X. Wang, J. Ding, Z. Xie, L. Wang, L. *Adv. Opt. Mater.* **2015**, *3*, 1349-1354; b) J. Liang, L. Ying, F. Huang, Y. Cao, *J. Mater. Chem. C* **2016**, *4*, 10993-11006.

[34] a) B. Ma P. I. Djurovich, S. Garon, B. Alleyne, M. E. Thompson, *Adv. Funct. Mater.* **2006**, *16*, 2438-2446; b) C. Shi, M. Huang, Q. Li, G. Xie, C. Yang, A. A. Yuan, *Dalton Trans.* **2018**, *47*, 17299-17303; c) M. Z. Shafikov, R. Daniels, P. Pander, F. B. Dias, J. A. G. Williams, V. N. Kozhevnikov, *ACS Appl. Mater. Interfaces* **2019**, *11*, 8182-8193.

10.1002/chem.202003571

WILEY-VCH

FULL PAPER

Entry for the Table of Contents

Sky-blue to yellowish-green OLEDs

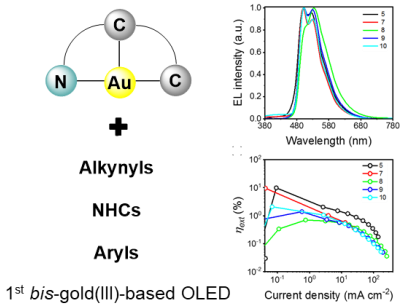

1st *bis*-gold(III)-based OLED

Organic light emitting diodes (OLEDs) have been successfully implemented in portable display devices, strongly competing with conventional large area displays and illumination sources. Efficient OLEDs have been fabricated using organometallic complexes of rare earth metals. However, the high material cost and low stability remain a central challenge for their implementation towards commercial display technologies. Gold(III) complexes are emerging as promising candidates as phosphorescent emitters. Herein, a series of novel gold(III) complexes stabilized by a κ^3-(N^C^C) bis-cyclometalated template, linked to various anionic ligands (alkynyl, NHC and aryl) was synthesized and applied to the fabrication of efficient solution-processable OLED materials. The color of emission is spanning from sky-blue (496 nm) to yellowish-green (544 nm), with EQE of up to 14%, showing the promising potential of such a pincer ligand to access stable phosphorescent gold(III) emitters.